Journal of Alloys and Compounds 509 (2011) 9679–9684

Contents lists available at ScienceDirect

Journal of Alloys and Compounds

journal homepage: www.elsevier.com/locate/jallcom

The diffusions and associated interfacial layer formation between thin film electrolyte and cermet anode in IT-SOFC

Zhi-Peng Li[a,*], Toshiyuki Mori[a], Graeme John Auchterlonie[b], Jin Zou[b,c], John Drennan[b], Masaru Miyayama[d]

[a] Global Research Center for Environment and Energy Based on Nanomaterials Science, National Institute for Materials Science, Tsukuba, Ibaraki 305-0044, Japan
[b] Centre for Microscopy and Microanalysis, The University of Queensland, St. Lucia, Brisbane, Queensland 4072, Australia
[c] Division of Materials, The University of Queensland, St. Lucia, Brisbane, Queensland 4072, Australia
[d] Research Center for Advanced Science and Technology, The University of Tokyo, Tokyo 153-8904, Japan

ARTICLE INFO

Article history:
Received 30 May 2011
Accepted 23 July 2011
Available online 29 July 2011

Keywords:
Transmission electron microscopy (TEM)
Diffusion
Interface
Grain boundaries
Electrophoretic deposition (EPD)
Solid oxide fuel cell (SOFC)

ABSTRACT

Dense 20 at.% gadolinium-doped (20GDC) thin film electrolyte supported by Ni–20GDC cermet anode has been fabricated by electrophoretic deposition technique. The microstructure and spatial distribution of constituent elements of this half-cell sample have been characterized by a combination of various techniques. The energy-dispersive X-ray spectroscopy (EDX) investigations, operated in scanning transmission electron microscopy (STEM) mode, illustrate that not only diffusion of metallic Ni from the anode into the electrolyte but also simultaneous counter-diffusion of Ce and Gd rare-earth cations from the electrolyte to the anode. Such mutual diffusion mainly occurs not only at the electrolyte–anode interface, but also occurs at the anode where Ni grains meet GDC grains. STEM high-angle annular dark-field (HAADF) imaging detects grain boundary segregation phenomena and suggests that grain boundaries can provide another possible pathway for diffusing atoms/ions. These investigations help explain the formation of an electrolyte–anode interfacial layer in terms of the mutual diffusion and diffusion along grain boundaries, and raise awareness of such diffusions that take place even during the process of cell sample preparation.

1. Introduction

Solid oxide fuel cells (SOFCs), as electrochemical energy conversion devices, have been widely accepted as promising candidates for new generation power systems due to their high efficiency, quiet operation and low or zero emission of pollutants [1,2]. Nevertheless the high operating temperature (around 1000 °C) of SOFCs limits the choice of materials and thus results in high cost of both cell materials and interconnect components, serious degradation, reduced longevity, and other technical problems [3,4]. In order to enhance the long-term performance stability, widen cell material selection and address relative technical issues, reducing the high operating temperature to intermediate range (500–600 °C) or even lower is crucial for current SOFC research [5,6]. Accordingly, it requires lower cell losses of the electrolyte yet still retains high power density that can be generally achieved at high operating temperatures. It is believed that alternative materials, like rare-earth-doped ceria with higher ionic conductivity than traditional yttria-stabilized zirconia (YSZ), have the potential to develop intermediate temperature SOFCs (IT-SOFCs) [2,7]. Take gadolinium-doped ceria (GDC) for example, its ionic conductivity is over one order of magnitude larger than that of YSZ at 500 °C (about 0.016 S cm^{-1} for GDC while only 0.0008 S cm^{-1} for YSZ) [8]. On the other hand, reducing the electrolyte thickness is another efficient way to overcome the increase in the area specific resistance of electrolyte operated at intermediate or low temperatures [9,10]. As the electrolyte thickness reduces, especially to the micrometer level, the role and influence of electrolyte–electrode interface become more significant.

Even though cells actually work at intermediate temperatures, high temperature treatment is still necessary for cell fabrication. Therefore, some interactions among cell components may occur, especially at electrolyte–electrode interfaces, which can influence both the mechanical and electrochemical properties of IT-SOFCs. It was reported that cathode material $LaSrCoO_3$ tended to react with YSZ electrolyte and form insulating materials (i.e., $La_2Zr_2O_7$ or $SrZrO_3$), resulting in a substantial loss in unit cell performance [11,12]. High resistivity material $SrLaGa_3O_7$ can also be formed due to the interaction between $La_{0.9}Sr_{0.1}Ga_{0.8}Mg_{0.2}O_{2.85}$ and GDC, and consequently increases the internal resistivity of SOFCs [13]. In addition to interactions, interdiffusions among cell components are by no means negligible. Sakai et al. [14] reported the

* Corresponding author. Tel.: +81 29 8513354x8544; fax: +81 29 8604712.
E-mail address: LI.Zhipeng@nims.go.jp (Z.-P. Li).

0925-8388/$ – see front matter © 2011 Elsevier B.V. All rights reserved.
doi:10.1016/j.jallcom.2011.07.080

reaction between cathode materials ($La_{0.8}Sr_{0.2}CoO_3$, $La_{0.8}Sr_{0.2}FeO_3$) and rare-earth-doped ceria in electrolyte, and the existence of a secondary phase that formed at electrolyte–cathode interface. Moreover, they found that a significant amount of transition metal would migrate or diffuse into doped ceria, whereas little migration of ceria or rare earth elements was observed [14]. In spite of extensive attention to such interactions or interdiffusions between cathode and electrolyte [15–17], there have been insufficient investigations on those phenomena at electrolyte–anode interface. This might be attributed to the fact that widely used SOFC anodes are mainly formed by metallic Ni mixed in ceramic polycrystals. Both YSZ and ceria are believed to exhibit good chemical compatibility with Ni and NiO [18]. Therefore, solid state reaction and interdiffusion between YSZ or ceria and Ni/NiO are not anticipated and thus rarely studied. However, our recent work illustrated that the interdiffusion between Ni and ceria at the electrolyte–anode interface should not be neglected. It was demonstrated that metallic Ni could diffuse from anode into the samarium-doped ceria or GDC electrolytes [19,20]. Furthermore, Ni diffusion may enhance the microstructural inhomogeneity and lead to the interfacial layer formation at the electrolyte–anode interface, which would decrease the conductivity of thin film electrolyte [19,20]. Similar to Sakai et al. work, previous studies detected only significant Ni diffusion but failed to observe any other migration/diffusion of ceria or doped rare-earth elements. Besides, due to the qualitative nature and spatial resolution of the energy-dispersive X-ray spectroscopy (EDX) operated in the scanning electron microscopy (SEM) mode, quantitative data about the interdiffusion is still lacking. Nevertheless, it is such quantitative data and the related diffusion mechanism that are critical to fabricate high quality electrolyte–electrode interface and hence worth further investigations.

The purpose of present work is to examine quantitatively interdiffusion phenomena occurring at both GDC thin film electrolyte and Ni–GDC cermet anode, especially at the interface between them. To approach this target, a combination of various types of techniques, such as SEM, transmission electron microscopy (TEM), energy-filtered TEM (EFTEM) and scanning TEM (STEM), are employed for comprehensive characterizations. The mechanisms of interdiffusion and other possible diffusions are discussed based on elemental distribution results obtained by EDX operated in STEM mode.

2. Experimental

For the fabrication of anode supported half-cell sample, 20 at.% GDC (20GDC) and commercial NiO powders were used for anode substrate preparation. The homogeneous 20GDC nanopowder was synthesized by ammonium carbonate co-precipitation method [21] and used as starting powders. NiO, 20GDC, and acetylene black were milled by zirconia balls in ethanol for successive 12 h with a rotation rate of 2 r/s. Immediately after ball milling, the slurry was dried in hot wind to avoid sedimentation. Such mixture was dried in N_2 overnight, and then mixed with PVA binder solution. After that, the mixture was dried again and sieved to fine powders, which was subsequently compacted into NiO–GDC green body by being isostatically pressed under 200 MPa. 20GDC nanopowders were dispersed in the suspension made of acetylacetone–iodine mixture and subsequently deposited directly onto the NiO–GDC substrate by electrophoretic deposition (EPD) technique [22]. Deposited thin films with different thickness can be obtained by tuning the voltage of direct current supply and deposition time. In this work, about 10 μm 20GDC thin film was deposited by carefully controlling the voltage of 10 V for successive 2 min during EPD process. The assembly of half-cell sample was then co-fired at 1400 °C in air for 6 h, and further heated at 600 °C for 2 h under following H_2 gas (50 mL/min) in order to fully reduce NiO into metallic Ni.

SEM (Hitachi S-5000) initially observed the cross-sectional morphology of half-cell samples. Then detailed microstructural features and microchemistry of such sample were characterized by a STEM (FEI Tecnai F30), operated at 300 kV and equipped with a Gatan imaging filter. Cross-sectional TEM samples for electrolyte–anode interface observations were prepared by traditional TEM sample preparation method: mechanical cutting, thinning, dimpling and final ion milling in a precision ion polishing system, operated at 4.5 keV with both guns at 10 μA in a sector pattern. EFTEM mapping was employed to investigate the spatial distribution of constituent elements at interfacial region. STEM can not only provide sample morphology and microstructures directly through bright-field (BF) imaging, but also qualitatively detect the spatial distributions of different elements in the sample by high-angle annular dark-field (HAADF) imaging. Unlike BF image formed by unscattered electrons and low angle dark-field (DF) image by Bragg scattered electrons, HAADF image was developed only by high angle incoherently scattered electrons. In the STEM HAADF imaging, the fine electron nanoprobe (around 5 nm used in this study) is scanned across electron-transparent thin area and those scattered electrons are then collected via the HAADF detector. Particularly, due to different scattered angles by different elements, the corresponding HAADF image will reveal different intensity directly related to the atomic number of constituent elements in the material. Therefore, the close connection with chemical contrast revealed in HAADF imaging renders it one of the most effective techniques for local characterization of heterogeneities and spatial distributions of various constituents. It was hence used in this study to identify locally distributed heterogeneities in the sample. The STEM was also employed in combination with EDX analysis to investigate quantitatively the one-dimensional elemental distribution of each constituent in the half-cell sample, especially across the electrolyte–anode interface. The profile size for STEM EDX line scan used in this study was 100 with dwelling time of 1.5 s.

3. Results

3.1. Mutual diffusion between Ni particles and GDC grains

Initial observations of the electrolyte–anode interfacial morphology of a half-cell sample was conducted by SEM. Fig. 1a is a clear representation of the well adhered dense thin film deposited on the porous Ni–GDC substrate by using EPD technique. The porous anode was produced by reducing initial NiO to metallic Ni particles through H_2 gas treatment, with the flowing rate of 50 mL/min at 600 °C for 2 h. The reduction treatment can help to obtain an electron conducting path percolating from the electrolyte toward the external circuit. It also helps to produce sufficient triple phase boundaries where electrochemical reactions usually occur [23]. The good adhesion of the thin film electrolyte on top of the porous anode substrate can be further revealed by an intermediate magnification SEM observation, as represented in Fig. 1b. The interfacial morphology of more detailed microstructural features was further characterized by TEM. The electrolyte–anode interface, between the dense electrolyte and porous substrate, can be easily seen in the TEM as shown in Fig. 1c. Fig. 1d is an EFTEM thickness map acquired by standard log-ratio method (coded in the Gatan DigitalMicrograph), and yielded the relative thickness of the sample. The porous substrate can be thinned faster than the dense electrolyte under the same Ar ions bombarding in ion-milling system. Therefore, the EFTEM thickness map represents the qualitative nature of the sample in terms of relative thickness as a result of different contrasts. The morphology of the electrolyte–anode interfacial region between dense GDC and porous Ni–GDC can be easily recognized as shown in Fig. 1d. EFTEM elemental maps (Fig. 1e and f) can also qualitatively demonstrate the spatial distributions of constituent elements at such interfacial region, which were zoomed in from the region denoted by the dashed square in Fig. 1d. Fig. 1e is Ni L edge (855 eV) EFTEM elemental map and Fig. 1f is the corresponding Ce M edge (883 eV) map of the same region. Note that at all sharp grain boundaries are no longer observable. Instead, there are considerable overlapping areas between contacted Ni and GDC grains, which indicates interdiffusions between Ni particles and GDC grains at such regions.

Quantitative detections of spatial distributions of constituent elements were consequently conducted by STEM EDX scans. Fig. 2a is a typical STEM DF image, from which dense film adhered to porous substrate can be recognized. This type of morphology is in accordance with what was observed by SEM and EFTEM in Fig. 1. The STEM EDX line scan was conducted exactly across the interface as labeled by the dashed line in Fig. 2a. Consistent with results of prior SEM EDX investigations [19,20], the concentration profile of STEM EDX result in Fig. 2b suggests that Ni in the anode site can diffuse into GDC grains in the electrolyte. However, some

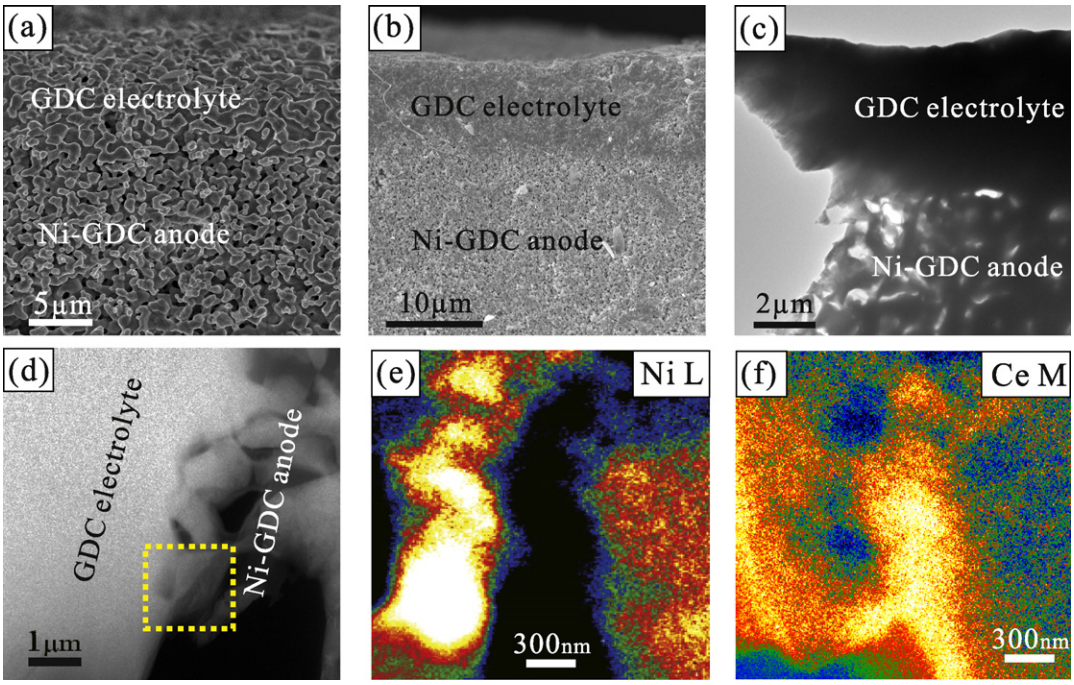

Fig. 1. The cross-sectional morphology of thin film electrolyte on porous anode substrate by SEM (a and b), TEM (c) and EFTEM (d) observations. EFTEM elemental maps of Ni and Ce are represented at (e) and (f) respectively, which are the magnified region that marked by the dashed square in (d).

interesting phenomenon was not captured or neglected in previous observations, that the rare earth elements Ce and Gd diffuse from the electrolyte into the metallic Ni particles in the anode. It was believed to be negligible in previous results [14,19,20]. Fig. 2b quantitatively displays that the mutual diffusion length at the interface is about 200 nm, revealing that a significant amount of Ni, Ce and Gd have inter-migrated. Fig. 2c and d show another example of STEM EDX investigation at the electrolyte–anode interfacial region of a new sample but prepared in the same method. The STEM BF image (Fig. 2c) represents and edge-on grain boundary of a Ni particle and its adjacent GDC grain. The STEM EDX line scan was conducted exactly across such an edge-on grain boundary. From the corresponding line scan profile (Fig. 2d), it can be noted that there is a mutual diffusion between the contacted Ni and GDC grains, with the mutual diffusion lengths of Ni, Ce and Gd over 200 nm. All other STEM EDX line scans (data are not shown here) statistically demonstrate that the mutual diffusion occurred at the electrolyte–anode interfacial region generally has an average diffusion length about 200 nm. Moreover, the equal diffusion length of all diffusing elements implies that such diffusion is independent of ionic radii. Previous reports showed that Ni diffusion from the anode into the electrolyte could lead to interfacial layer formation [19,20]. Therefore, the results represented in Figs. 2b and d also suggest that counter-diffusing of Ce/Gd cations can play the same role as diffusing Ni. In other words, such mutual diffusion zone, with the mixture of diffused Ni, Ce and Gd ions, can be assigned to the interfacial layer formation at the electrolyte–anode interface.

It is worth noting that, there is no specific chemical difference between Ni–GDC borderland at electrolyte–anode interface and Ni–GDC grain boundary in anode, due to the same chemical composition of all GDC gains in both electrolyte and anode. Based on observations of mutual diffusion among Ni, Ce, and Gd occurring at the electrolyte–anode interface, it is thereby anticipated that such mutual diffusion can also be detected between Ni particles and GDC gains at the anode site. Fig. 2e is the STEM DF image of Ni particles and GDC grains observed in the anode. The STEM EDX line scan, conducted across the edge-on grain boundary denoted in Fig. 2e, confirms the existence of mutual diffusion between metallic Ni particle and GDC grain in anode. However, the corresponding mutual diffusion length is only about 90 nm. Other STEM EDX detections also show that the average mutual diffusion length at the anode site is less than 100 nm, much shorter than that at the electrolyte–anode interface. The discrepancy of mutual diffusion length will be discussed later.

3.2. Diffusion along grain boundaries

Since mutual diffusions mainly occur at electrolyte–anode interfacial region, it is prudent to investigate other possible diffusion pathway for all constituent elements that may exist among cell components. Fig. 3a is the STEM BF micrograph of grains near the electrolyte–anode interface, from which microstructural features of such as grain boundaries can be clearly seen. In order to obtain the information of elemental distribution, especially at grain boundary region, HAADF imaging technique was used. Fig. 3b is the corresponding HAADF image of Fig. 3a. Elements with different atomic numbers will exhibit different contrast in HAADF micrograph, which provides an intuitional way to investigate the spatial distribution of different elements. The enhanced contrast at grain boundaries (marked by dashed ellipses in Fig. 3b) in HAADF image implies that there are elements segregating along grain boundaries that are different from those in neighboring grain interiors. Such grain boundaries with enhanced bright contrast in HAADF image can be widely observed at the interfacial region, in both electrolyte and anode sites. Considering the aforementioned mutual diffusion, it is reasonable to assume another possible diffusion way that may also exist in the sample.

In order to identify the segregation phenomenon of grain boundary, the quantitative technique, STEM EDX analysis, was then employed. Fig. 4a is a STEM BF image of the anode site obtained near the electrolyte–anode interface. Initial STEM EDX points scan investigations can directly detect the composition of each grain as labeled in Fig. 4a. Similar to Fig. 3b, the corresponding STEM HAADF micrograph also indicates that different compositions may exist at the grain boundary of two contacted Ni particles, reflected by the brighter contrast. According to the concentration profile

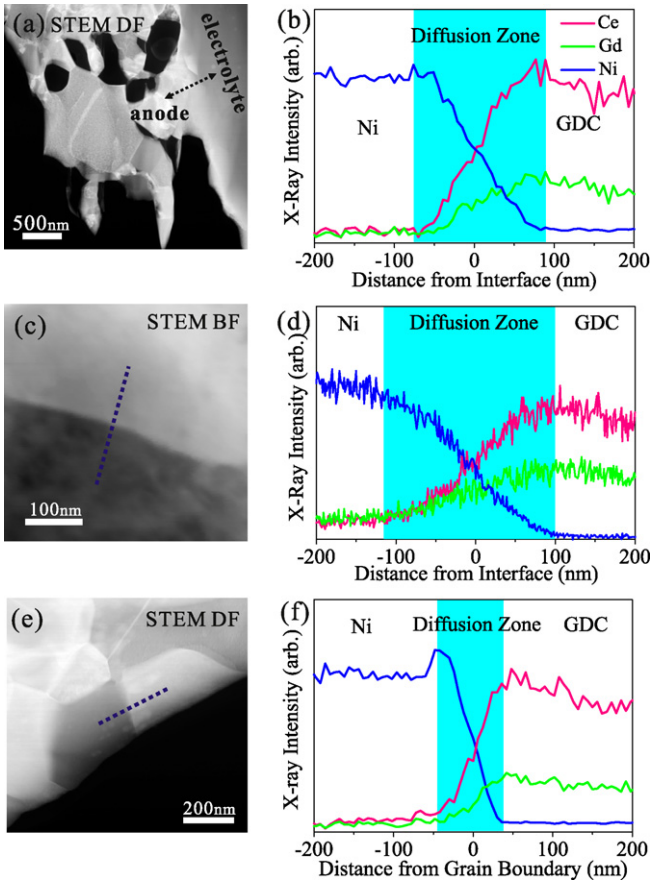

Fig. 2. (a) STEM DF image of the morphology of electrolyte–anode interface and (b) the corresponding concentration profile of STEM EDX line scan across the interface as denoted by the dashed line in (a). STEM BF images of microstructures of adjacent grains at the electrolyte–anode interface and the anode site are shown in (c) and (e) respectively. (d and f) Corresponding concentration profiles of STEM EDX line scans across edge-on grain boundaries as labeled by the dashed line in (c) and (e) separately.

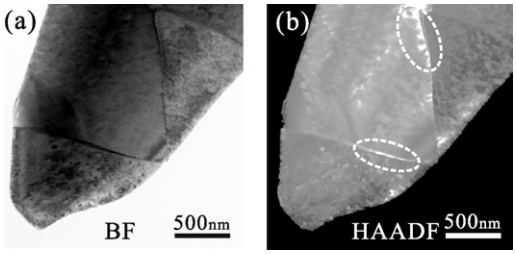

Fig. 3. (a) STEM BF image of adjacent grains near the electrolyte–anode interface and (b) the corresponding STEM HAADF image showing enhanced brightness at grain boundaries.

of STEM EDX line scan, Ce and Gd are enriched at the Ni grain boundary. Based on the morphology shown in STEM images (Fig. 4a and b), such segregation of Ce and Gd can be attributed to Ce/Gd diffusion from nearby GDC grains. It suggests that the grain boundary can provide another possible pathway for elements diffusion, which is highlighted by two dashed arrows in Fig. 4b. This scenario was verified by statistical detections of grain boundary segregation and diffusion adjacent to the electrolyte–anode interfacial region through STEM EDX analyses.

Differ from the mutual diffusion with an average diffusion length around 200 nm at the electrolyte–anode interfacial region; the diffusion along the grain boundary seems much longer in length. Following the same procedures discussed before, STEM EDX

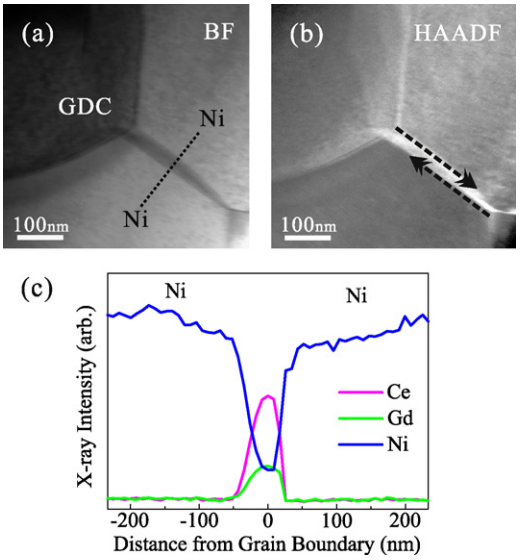

Fig. 4. (a) STEM BF image of several contacted grains at the anode but near the electrolyte–anode interface, the corresponding STEM HAADF image is shown in (b). The possible diffusion pathway along the grain boundary is denoted by dashed arrows in (b). (c) The concentration profile of STEM EDX line scan across the grain boundary as marked in (a).

point scan was conducted first to distinguish metallic Ni particles and GDC grains at the anode site. STEM EDX line scans were then acquired between Ni particles near the electrolyte–anode interface. It was found that segregation of diffused cations (Ce and Gd) along grain boundary could be detected (as shown in Fig. 5a) to be located at about 1 μm away from the electrolyte–anode interface. However, it is difficult to prove directly that such segregated Ce and Gd cations actually diffused from the electrolyte, since there are plenty of GDC grains in anode and similar diffusions along grain boundary from other anode GDC grains may also occur. Therefore, comparative STEM EDX analyses were conducted at electrolyte site. Fig. 5b is another typical STEM EDX line scan acquired at the electrolyte site. The concentration profile clearly demonstrates the considerable segregation of metallic Ni at the boundary of two adjacent GDC grains. Since there are no Ni particles in the electrolyte at all, the metallic Ni detected in electrolyte must have originated from Ni diffusion from the anode along grain boundaries. This thereby provides an indirect way to investigate the diffusion along grain boundary, and verifies that diffusion along grain boundary is easier or faster than mutual diffusion between contacted Ni particles and GDC grains at the electrolyte–anode interface.

4. Discussion

STEM EDX analyses reveal that both Ni and GDC can mutually diffuse into each other at both electrolyte–anode interface and the anode site. Besides such mutual diffusion, Ni, Ce and Gd can diffuse along grain boundaries around the interfacial region. Even though there are distinct differences in the radii of diffusing atoms/ions, they have equal diffusion length. Hence, such mutual diffusion can be considered as a substitution diffusion, which is quite different from the interstitial cation diffusion that dominates the grain boundary mobility in doped ceria systems [24]. It is believed that such mutual diffusion will subsequently lead to the formation of mutual diffusion zone with the mixture of diffused Ni, Ce and Gd atoms/ions. By comparing mutual diffusion between Ni particles and GDC grains detected at the electrolyte–anode interface with that at anode site, it was found that the former has longer average diffusion length (~200 nm) than the latter (<100 nm). Chemically, since there is no difference between Ni/GDC grains at

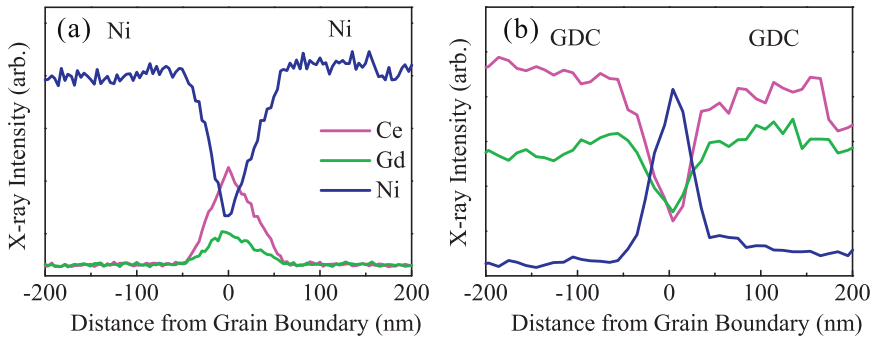

Fig. 5. Comparison of STEM EDX profiles across the grain boundary of (a) two contacted Ni particles in the anode site and (b) two contacted GDC grains in the electrolyte site. Both detected grain boundaries are near the electrolyte–anode interface.

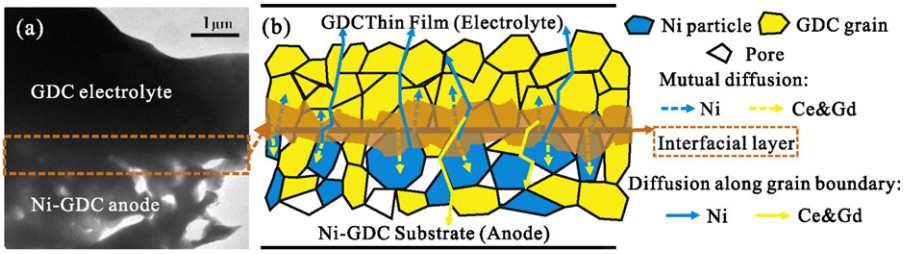

Fig. 6. (a) TEM BF image of the morphology of electrolyte–anode interface and (b) schematic diagram of the interfacial layer formation induced by both mutual diffusion and diffusion along grain boundaries at the electrolyte–anode interfacial region.

the electrolyte–anode interface and those at the anode site, it is necessary to explain such discrepancy in mutual diffusion length from other perspectives, e.g., the geometric difference. At atomic level, the mutual diffusion actually occurs across the respective boundaries between Ni particles and GDC grains. Diffusing atoms/cations should migrate from one grain to the neighboring one through the direct contact area, i.e., the neck of contacting grains. Such 'neck' diffusion will be strongly affected by the geometric differences as the size and density of contact areas. Due to the porosity of the anode substrate, the grain density in the anode is much lower than that in the dense thin film. Accordingly, the average contact areas between Ni particles and GDC grains at the electrolyte–anode interface are much larger than those at the anode site. This geometric discrepancy will consequently enhance the mutual diffusion intensity, motivate additional diffusion through nearby contacted areas, and result in longer average mutual diffusion length detected at the electrolyte–anode interface.

Based on our observations of mutual diffusion and segregation/diffusion along grain boundaries, we hence rationalize the diffusion phenomena and interfacial layer formation as demonstrated in Fig. 6. Fig. 6a is a representative TEM BF image of the electrolyte–anode interfacial morphology, and Fig. 6b is the schematic diagram of the interfacial layer formation at this interface. Similar to previous results, Ni can diffuse into GDC grains from anode to electrolyte. Simultaneously, counter-diffusion of Ce and Gd into metallic Ni particles will also occur. Such mutual diffusion will lead to the mutual diffusion zone formation with the mixture of diffused Ni, Ce and Gd ions. This evolution in composition at the electrolyte–anode interface is believed to affect the electrical/ionic properties of the cell components [25]. Despite identified equal diffusion length of diffusing ions, due to distinct ionic radius differences, a broad solubility range between metallic Ni and GDC is not anticipated. On the other hand, grain boundary segregation near the electrolyte–anode interface detected by STEM EDX investigations exhibits a tendency for constituent elements to diffuse along grain boundaries among cell components. With large volume of boundary vacancies and associated defects, the grain boundary can serve as a trapping center that provides enough voids to accommodate diffusing atoms/ions [26]. This process can thus provide another pathway for atoms/cations diffusion near the electrolyte–anode interfacial region. The diffusion along the grain boundary is assumed easier and faster than the mutual diffusion, which is verified by the STEM EDX analyses. Therefore, two types of diffusions can be clarified, which is believed to motivate the interfacial layer formation at the electrolyte–anode interface. Since it is well established that the actual reactive zone for hydrogen–oxygen reaction exists within a limited region at the anode in SOFCs, approximately 10 μm near the electrolyte–anode interface [27], the interfacial layer formation will have considerable influence and subsequently degrade SOFCs characteristics. For example, it was reported that such interfacial layer would result in reduced ionic conductivity of electrolyte thin film [19].

One more thing needs to be noted that, such mutual diffusion and diffusion along grain boundaries actually occurred during cell preparation. It draws our attention to the unexpected interfacial layer formation at the electrolyte–anode interface even before cell operation. Therefore, in order to prepare high quality cells, especially high quality of electrolyte–electrode interface, more precautions should be paid during cell preparation process. Such mutual diffusion as well as the diffusion along grain boundaries is also expected to continue during cell operation, which will have a strong impact on the performance of SOFCs. Note that it is quite difficult to avoid such diffusions at atomic level, since high temperature treatment is necessary for cell preparation even when operating temperature is low. Nevertheless, insights from this study can still motivate us take other perspectives. For example, we may make use of such diffusions by choosing beneficial materials so that the mutual diffusion zone can be formed with more active sites taking place, which can enhancement the performance of SOFCs.

5. Conclusions

In the study, the microstructures and spatial distributions of constituents in GDC thin film electrolyte and Ni–GDC cermet anode

of a half-cell sample have been comprehensively characterized by a combination of various techniques (i.e., SEM, TEM, EFTEM mapping, STEM HAADF imaging and STEM EDX). Two types of diffusions, the mutual diffusion and the diffusion along grain boundaries, have been detected and clarified. Initial investigation by EFTEM mapping qualitatively shows that there is a considerable interdiffusion zone between directly contacted Ni particles and GDC grains at the electrolyte–anode interface. Quantitative STEM EDX analyses identify not only the diffusion of Ni diffuse from anode into the GDC electrolyte (as previously reported [19,20]) but also that of rare-earth elements Ce and Gd from electrolyte into metallic Ni in the anode. Moreover, all the diffusing elements have equal diffusion length despite their significant differences in ionic radii, which indicates that substitution diffusion is the dominant mechanism in the mutual diffusion at the electrolyte–anode interface. Due to geometric discrepancies among cell components, such mutual diffusion mainly occurred at the electrolyte–anode interface rather than in the anode. Besides the mutual diffusion, diffusing elements were detected to segregate along grain boundaries near the electrolyte–anode interfacial region. It suggests that grain boundaries can provide a possible pathway for Ni, Ce and Gd diffusion, and was verified to be an easier and faster diffusion way than the mutual diffusion. As such, the interfacial layer formation at the electrolyte–anode interface was elucidated in terms of the mutual diffusion associated with the diffusion along grain boundaries. These investigations provide valuable insight into the mechanism of diffusions at the electrolyte–anode interfacial region. Additionally, the formation of this interfacial layer during cell sample preparation has considerably negative effects on the IT-SOFC performance because of low ionic conductivity and should be avoided.

Acknowledgements

This work was supported by the Grant-in-Aid for Scientific Research 22310053 from the Ministry of Education, Culture, Sports, and Technology (MEXT), Japan. The authors also appreciate the partial funding support from Global Research center for Environment and Energy based on Nanomaterials science (GREEN), National Institute for Materials Science, Japan. G.J. Auchterlonie also expresses his thanks for the financial support from the Australian Academy of Sciences – Japan Society for the Promotion of Science Bilateral Exchange Program, scientific visits to Japan (2010-2011-RC 21001001).

References

[1] B.C.H. Steel, A. Heinzel, Nature 414 (2001) 345–352.
[2] N.Q. Minh, J. Am. Ceram. Soc. 76 (3) (1993) 563–588.
[3] M. Dokiya, Solid State Ionics 152 (2002) 383–392.
[4] S.M. Haile, Acta Mater. 51 (2003) 5981–6000.
[5] B.C.H. Steele, Solid State Ionics 134 (2000) 3–20.
[6] D.J.L. Brett, A. Atkinson, N.P. Brandon, S.J. Skinner, Chem. Soc. Rev. 37 (2008) 1568–1578.
[7] S.J. Hong, K. Mehta, A.V. Virka, J. Electrochem. Soc. 145 (1998) 638–647.
[8] H. Inaba, H. Tagawa, Solid State Ionics 83 (1996) 1–16.
[9] S.D. Souza, S.J. Visco, L.C. De Jonghe, Solid State Ionics 98 (1997) 57–61.
[10] D. Beckel, A.B. Hutter, A. Harvey, A. Infortuna, U.P. Muecke, M. Prestat, J.L.M. Rupp, L.J. Gauckler, J. Power Sources 173 (2007) 325–345.
[11] T. Kawada, N. Sakai, H. Yokokawa, M. Dokiya, I. Ansai, Solid State Ionics 50 (1992) 189–196.
[12] A. Tsoga, A. Gupta, A. Naoumidis, P. Nikolopoulos, Acta Mater. 48 (2000) 4709–4714.
[13] M. Hrovat, A.A. Khanlou, Z. Samardzija, J. Holc, Mater. Res. Bull. 34 (1999) 2027–2034.
[14] N. Sakai, H. Kishimoto, K. Yamaji, T. Horita, M.E. Brito, H. Yokokawa, J. Electrochem. Soc. 154 (12) (2007) B1331–B1337.
[15] M.J.L. Ostergard, C. Clausen, C. Bagger, M. Mogensen, Electrochim. Acta 40 (12) (1995) 1971–1981.
[16] A. Mitterdorfer, L.J. Gauckler, Solid State Ionics 111 (1998) 182–218.
[17] A. Grosjean, O. Sanseau, V. Radmilovic, A. Thorel, Solid State Ionics 177 (2006) 1977–1980.
[18] S. Primdahl, M. Mogensen, Solid State Ionics 152 (2002) 597–608.
[19] D.R. Ou, T. Mori, F. Ye, M. Miyayama, S. Nakayama, J. Zou, G.J. Auchterlonie, J. Drennan, J. Electrochem. Soc. 156 (7) (2009) B825–B830.
[20] F. Ye, T. Mori, D.R. Ou, J. Zou, J. Drennan, S. Nakayama, M. Miyayama, Solid State Ionics 181 (2010) 646–652.
[21] Z.P. Li, T. Mori, G. Auchterlonie, J. Zou, J. Drennan, Appl. Phys. Lett. 98 (094104) (2011) 1–3.
[22] S. Nakayama, M. Miyayama, Key Eng. Mater. 350 (2007) 175–178.
[23] W. Guo, J. Liu, Solid State Ionics 179 (2008) 1516–1520.
[24] P.L. Chen, I.W. Chen, J. Am. Ceram. Soc. 79 (1996) 1793–1800.
[25] A. Naoumidis, A.A. Khanlou, Z. Samardzija, D. Kolar, Fresenius J. Anal. Chem. 365 (1999) 277–281.
[26] G. Jung, T. Huang, J. Mater. Sci. 38 (2003) 2461–2468.
[27] R.E. Williford, L.A. Chick, G.D. Maupin, S.P. Simner, J.W. Stevenson, J. Electrochem. Soc. 150 (8) (2003) A1067–A1072.